View metadata, citation and similar papers at core.ac.uk

brought to you by CORE

provided by Elsevier - Publisher Connector

NEOPLASIA
www.neoplasia.com

Volume 12 Number 5 May 2010 pp. 397–404 397

Three-dimensionally Specific Inhibition of DNA Repair–Related Genes by Activated KRAS in Colon Crypt Model[1,2]

Toshiyuki Tsunoda[*,†,3], Yasuo Takashima[*,†,3], Takahiro Fujimoto[*,†], Midori Koyanagi[*,†], Yasuhiro Yoshida[*], Keiko Doi[*,†], Yoko Tanaka[*,†], Masahide Kuroki[†], Takehiko Sasazuki[‡] and Senji Shirasawa[*,†]

*Department of Cell Biology, Faculty of Medicine, Fukuoka University, Fukuoka, Japan; †Center for Advanced Molecular Medicine, Fukuoka University, Fukuoka, Japan; ‡International Medical Center of Japan, Tokyo, Japan

Abstract

Growth and differentiation of colonic epithelium are regulated in the three-dimensional (3D) physiological architecture, colonic crypt, and deregulation of 3D interactions is involved in tumorigenesis. Cell-based 3D culture systems provide a suitable approach bridging the gap between two-dimensional (2D) culture and animal models. *KRAS* mutations are found at high frequencies in human colorectal cancer (CRC); however, KRAS-targeted cancer therapy has not been developed. Here, we have established a 3D cell culture model resembling the colonic crypt by use of HKe3 cells, human CRC HCT116 cells disrupted at activated *KRAS*. In this 3D colonic crypt model, HKe3 cells showed the features of time course–dependent transit-amplifying and terminal-differentiated stages, which are characteristic of normal colonic crypt. On the basis of the features of HCT116 cells, activated KRAS inhibited normal cell polarity and apoptosis in 3D culture. The expression of DNA repair–related tumor suppressor genes including *TP53*, *BRCA1*, *BRCA2*, and *EXO-1* was markedly suppressed by activated KRAS in 3D culture but not in 2D culture. These results together suggest that activated KRAS plays critical roles in the accumulation of genetic alterations through inhibition of DNA repair genes and apoptosis and that this 3D culture model will provide a useful tool for investigating the molecular mechanisms of CRC development.

Neoplasia (2010) 12, 397–404

Introduction

Both cell-cell and cell-extracellular matrix interactions are critically involved in developmental programs and provide three-dimensional (3D) architectures *in vivo* [1], and deregulations of these interactions are frequently observed in cancer [2]. Because cells grown in traditional flat two-dimensional (2D) culture often differ in morphology, cell-cell interactions, and differentiation from the cells grown in physiological 3D environments [3,4], cell-based *in vitro* 3D culture systems provide a suitable approach that can bridge the gap between traditional 2D cell culture and animal models [2,5]. Human cancers are derived from epithelial tissues characterized by specific cellular architectures including epithelial cell-cell junctions, which allow the separation of apical and basolateral membranes. This apical-basal cell polarity is crucial in normal cell functions, and loss of cell polarity is a critical step in tumorigenesis [6–8].

Colonic epithelium makes a 3D structure called colonic crypt, where epithelial cells migrate upward through the transit-amplifying (TA) zone in the lower-to-middle region of the crypt, before becoming terminally differentiated (TD), and are eventually shed into the lumen [9]. Because most cell proliferation takes place in the TA region and terminal differentiation occurs distal to this region [9], a 3D culture model resembling colonic crypt should be needed for understanding the colorectal tumorigenesis *in vivo*.

Address all correspondence to: Senji Shirasawa, MD, PhD, Department of Cell Biology, Faculty of Medicine, Fukuoka University, 7-45-1 Nanakuma, Jonan-ku, Fukuoka 814-0180, Japan. E-mail: sshirasa@fukuoka-u.ac.jp

[1]This work was supported in part by the grant from the Ministry of Education, Culture, Sports, Science and Technology, Japan.

[2]This article refers to supplementary materials, which are designated by Figures W1 and W2 and Tables W1 to W4 and are available online at www.neoplasia.com.

[3]These authors contributed equally to this work.

Received 17 January 2010; Revised 15 February 2010; Accepted 16 February 2010

Copyright © 2010 Neoplasia Press, Inc. All rights reserved 1522-8002/10/$25.00

DOI 10.1593/neo.10170

Tumorigenesis is a multistep process in which genetic alterations accumulate, culminating in neoplastic phenotype [10–12]. In the adenoma-carcinoma sequence model of colorectal cancer (CRC) cell, adenomatous polyposis coli gene mutations occur in the first step, followed by particular mutations of oncogenes and tumor suppressor genes, along with genetic instability [11,13–15]. *KRAS* mutations are frequently observed not only in CRC but also in colorectal adenomas and in pancreatic and lung cancers [16–18]. Oncogenic mutations in *RAS* are invariably point mutations that either interfere with Ras GAP binding or directly disrupt Ras GTPase activity, locking RAS in a constitutively active form [16]. However, KRAS-targeted therapy has not been clinically developed, and patients with CRC bearing activated *KRAS* did not benefit from cetuximab, a monoclonal antibody against the epidermal growth factor receptor [17]. Elucidation of the precise molecular mechanisms of activated KRAS *in vivo* should be needed for the design and development of cancer therapies.

We and colleagues reported much about activated KRAS functions through comparing human CRC HCT116 cells and HKe3 cells, HCT116 cells disrupted at activated *KRAS* [19–22]. Here, we have established *in vitro* a 3D culture model resembling colonic crypt using HKe3 cells and elucidated the relation between activated KRAS and 3D architectures and functions comparing with HCT116 cells.

Materials and Methods

Cell Culture

2D culture for HCT116 cells, HKe3 cells, and e3-MKRas#14 cells and for HKe3-derived stable transfectants expressing activated KRAS was done as described previously [19,23]. A total of 5×10^5 cells were cultured in 10-cm culture dishes (Nunc, Rochester, NY) [19]. For the 3D cell culture, 8×10^3 cells were cultured in LabTek 8-chamber slides (Nunc) using Matrigel, a reconstituted basement membrane (BD Biosciences, San Jose, CA), as described previously [24] and according to the protocol online at http://brugge.med.harvard.edu/. Briefly, Matrigel was thawed overnight at 4°C, and 25 μl per well was spread over the surface of well on ice, followed by incubation at 37°C for 1 hour. Cells were seeded in the medium containing 2% (vol/vol) Matrigel. Half of the medium was replaced with fresh medium containing 2% Matrigel every 3 days.

Immunofluorescence Labeling and Confocal Microscopy

Immunofluorescence experiment was done as described previously [25]. Briefly, cells in the 3D culture were fixed using 3.7% formaldehyde in PBS and incubated at room temperature for 20 minutes. Permeabilization was done using 0.05% saponin, and the fixed cells were incubated at room temperature for 30 minutes. Blocking was done by PBS containing 10% normal goat serum (Jackson ImmunoResearch, West Grove, PA) at 4°C for 1 hour, followed by incubation of primary antibodies in blocking buffer for 15 hours at 4°C. The wells were washed three times with PBS containing 0.5% NP-40 and twice with PBS, followed by incubation of Alexa-conjugated secondary antibodies (Invitrogen, Carlsbad, CA) diluted in blocking buffer to 1:200 for 1 hour at room temperature. The wells were rinsed as described here, and 50 μl of ProLong Gold antifade reagent (Invitrogen) was added. Primary antibodies used were cleaved caspase-3 (5A1; Cell Signaling Technology, Beverly, MA), laminin-5 (D4B5; Millipore, Billerica, MA), ZO-1 (1/ZO-1; BD Biosciences, San Jose, CA), and Ki-67 (Thermo Scientific, Rockford, IL). Alexa Fluor 568–conjugated to phalloidin (Invitrogen) and 4′,6-diamidino-2-phenylindole (DAPI; Sigma-Aldrich, St Louis, MO) were used for staining of F-actin and DNA, respectively. For the examination of 3D structures, TCS-SP5 Laser Scanning confocal microscopy (Leica, Wetzlar, Germany) was used. The figures show the representative data from three independent experiments.

Quantification of Apoptosis in 3D Structures

HCT116 and HKe3 cells were cultured for 6 days in Matrigel and were stained by anti–cleaved caspase-3 antibody and DAPI at day 6. Cleaved caspase-3–positive cells were counted in a cross section of the 3D culture at maximum diameter, and the 3D structure containing more than two positive cells were defined as apoptotic. The 3D structures for HCT116 and HKe3 cells were analyzed in three independent experiments, and the average ratio of apoptotic 3D structure was calculated.

Quantification of Proliferative Cells Grown in 3D Culture

HCT116 and HKe3 cells were cultured for 6 days in Matrigel and were stained by anti–Ki-67 antibody and DAPI at the indicated day from day 1 to day 6. The ratio of Ki-67–positive cells in the total cells contacting Matrigel in the cross section of 3D structures at maximum diameter was calculated. Similar results were obtained from independent experiments.

Expression Microarray Analysis

Total RNA from cells cultured in the 2D or 3D cultures were extracted as described previously [26]. Gene expression arrays were done using Human Genome U133 Plus 2.0 Array 6800 GeneChips (Affymetrix, Santa Clara, CA) and were analyzed by GeneSpring v7.3 software (Agilent Technologies, Santa Clara, CA) as previously described [26].

Real-time Quantitative Reverse Transcription–Polymerase Chain Reaction

Real-time quantitative reverse transcription–polymerase chain reaction was done by Perfect Real-time Support System (Takara Bio, Inc, Shiga, Japan) for *BRCA1* (HA113973), *BRCA2* (HA119560), *EXO1* (HA104791), *TP53* (HA092869), *CTNNB1* (HA115708), and *ACTB* (HA067803). Complementary DNA were synthesized from total RNA as described previously [26]. Assays were performed on QuantiTect SYBR Green PCR Kits (Qiagen, Valencia, CA) and ABI PRISM 7900HT (Applied Biosystems, Foster City, CA), and *ACTB* values were used for normalization. The normalized values were quantified by the $\Delta\Delta C_t$ method and presented as means ± SDs for triplicate samples as described previously [27,28]. Each relative expression unit (REU) was determined by the REU of HCT116 in 2D culture as 1.0.

Western Blot Analysis

Western blot analysis was performed as described previously [29]. Cells grown in 3D culture were harvested by cold PBS with 5 mM EDTA, and Matrigel was separated by centrifugation, followed by cell lysis in RIPA buffer. Lysates were spun at 12,000 rpm at 4°C for 10 minutes, and the supernatants were quantified using Bradford ULTRA (Expedeon, San Diego, CA). The antibodies used were p53 (DO-1; Santa Cruz Biotechnology, Santa Cruz, CA) and ERK1 (K-23; Santa Cruz Biotechnology). The figures show the representative blot from three independent experiments. Quantitative Western blot analysis of p53 was performed using a measurement module (BZ-H1M; Keyence, Osaka, Japan) for obtaining integration values of each blot ($n = 3$). ERK1 intensity was used as the standard. The relative intensity of each signal

was normalized by the signal intensity in HKe3 cells grown in 3D culture as 1.0.

Statistical Analysis

Data were presented as mean ± SDs of means of triplicate samples. Statistical analysis was performed with an unpaired Student's *t*-test to compare the means of multiple groups. Differences at $P < .05$ are considered to be statistically significant.

Results

HKe3 Cells in 3D Culture Showed Cell Polarity and Luminal Cavity Formation

To elucidate the precise functions of activated KRAS in colorectal tumorigenesis, we compared the 3D structures between HKe3 and HCT116 cells grown in 3D cell culture using Matrigel containing laminin and collagen. To address the KRAS functions in 3D culture, morphological structure and apical-basal cell polarity were examined. Firstly, we examined the distribution of laminin V and F-actin, markers for basement membrane and apical membrane, respectively, in the HCT116 and HKe3 cells grown in 3D culture at day 6. Serial cross-sectional images from bottom to top showed that HKe3 cells formed a single layer of polarized cells and luminal cavity, where laminin V was placed at the basal region and F-actin was localized in the apical region (Figure 1*A*, *from left to right*). Conversely, localizations of laminin V and F-actin for HCT116 cells were disorganized, and luminal cavity was not observed (Figure 1*A*), indicating the loss of apical-basal cell polarity in HCT116 cells in the 3D culture. To further address cell polarity in the 3D culture, we examined the distribution of ZO-1, a tight junction marker. ZO-1 signals were localized at the border between the apical and basolateral membranes adjacent to luminal cavity of HKe3 cells but not in the HCT116 cells (Figure 1*B*), and distributions of ZO-1 and F-actin were colocalized in the HKe3 cells in the 3D culture (Figure W1), suggestive of the existence of normal apical-basal cell polarity in the HKe3 cells. Furthermore, e3-MKRas#14 cells, HKe3-derived stable transfectants expressing activated KRAS [23], showed impaired cell polarity or luminal cavity formation like HCT116 cells (Figure W2, *A* and *B*). These results together suggest that activated KRAS disturbs cell polarity and luminal cavity formation in the 3D culture.

Apoptosis in Luminal Epithelium of HKe3 Cells in 3D Structures

Apoptosis is induced by detaching from the surrounding extracellular matrix, called anoikis, in the luminal epithelial cells *in vivo* [30]. To address whether activated KRAS influences apoptosis in the 3D culture, we examined the apoptosis activity in the HCT116 and HKe3 cells

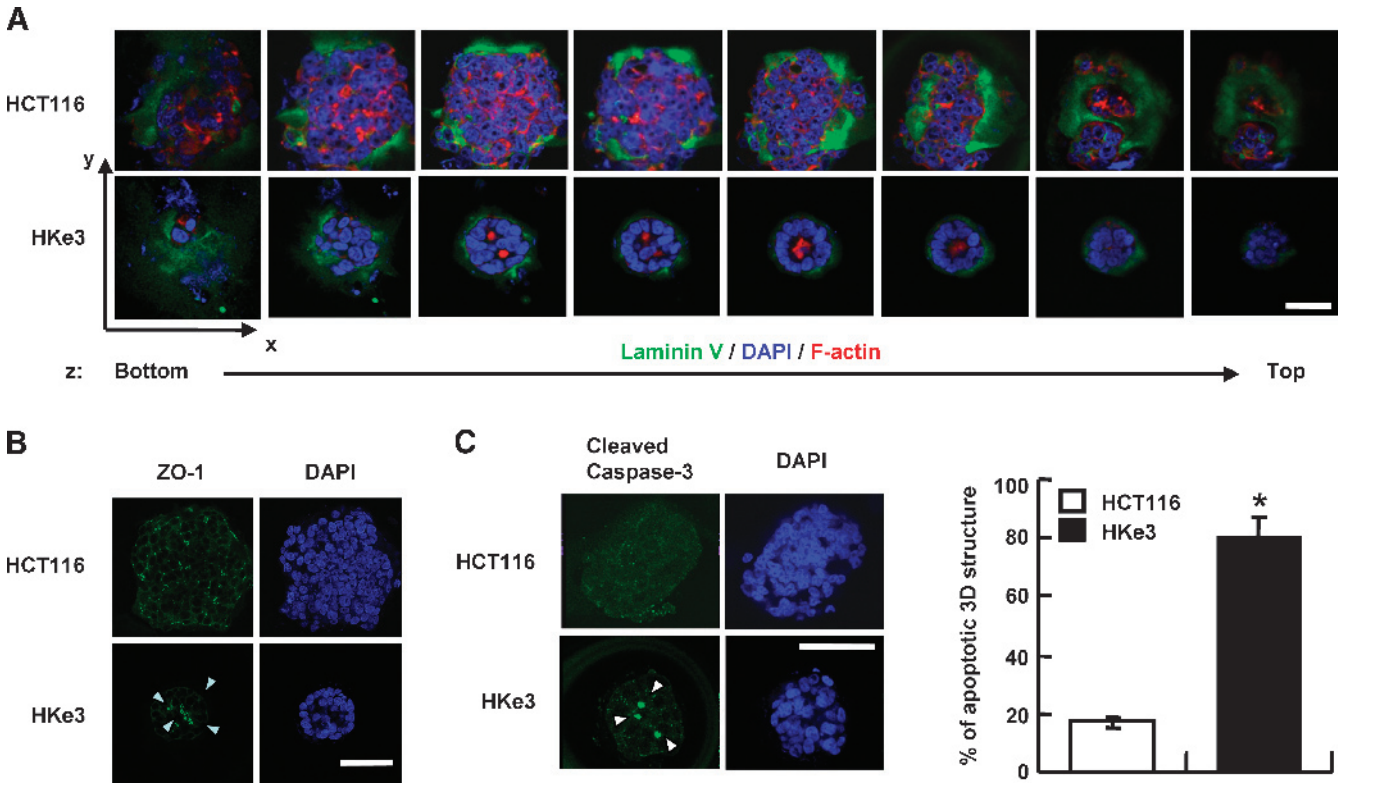

Figure 1. Activated KRAS is involved in loss of cell polarity, luminal cavity formation, and apoptosis. (A) Loss of apical-basal cell polarity by activated KRAS. Serial cross-sectional (*x-y* plane) images of the 3D spherical structures were displayed in every 3-μm distance (*z* axis). Red, F-actin; blue, nuclear DNA; green, laminin V. Bar, 25 μm. (B) Disruption of tight junctions by activated KRAS. Arrowhead indicates the ZO-1 signal. Blue, nuclear DNA; green, ZO-1. Bar, 50 μm. (C) Inhibition of apoptosis by activated KRAS. HCT116 and HKe3 cells in the 3D structures at day 6 were stained with DAPI (blue) and antibodies to the cleaved caspase-3 (green; left). Arrowhead indicates the cleaved caspase-3 signal. DAPI, blue; cleaved caspase-3, green. Bar, 50 μm. The ratio of the apoptotic 3D structures was shown (right). White bar, HCT116; black bar, HKe3. *$P < .001$.

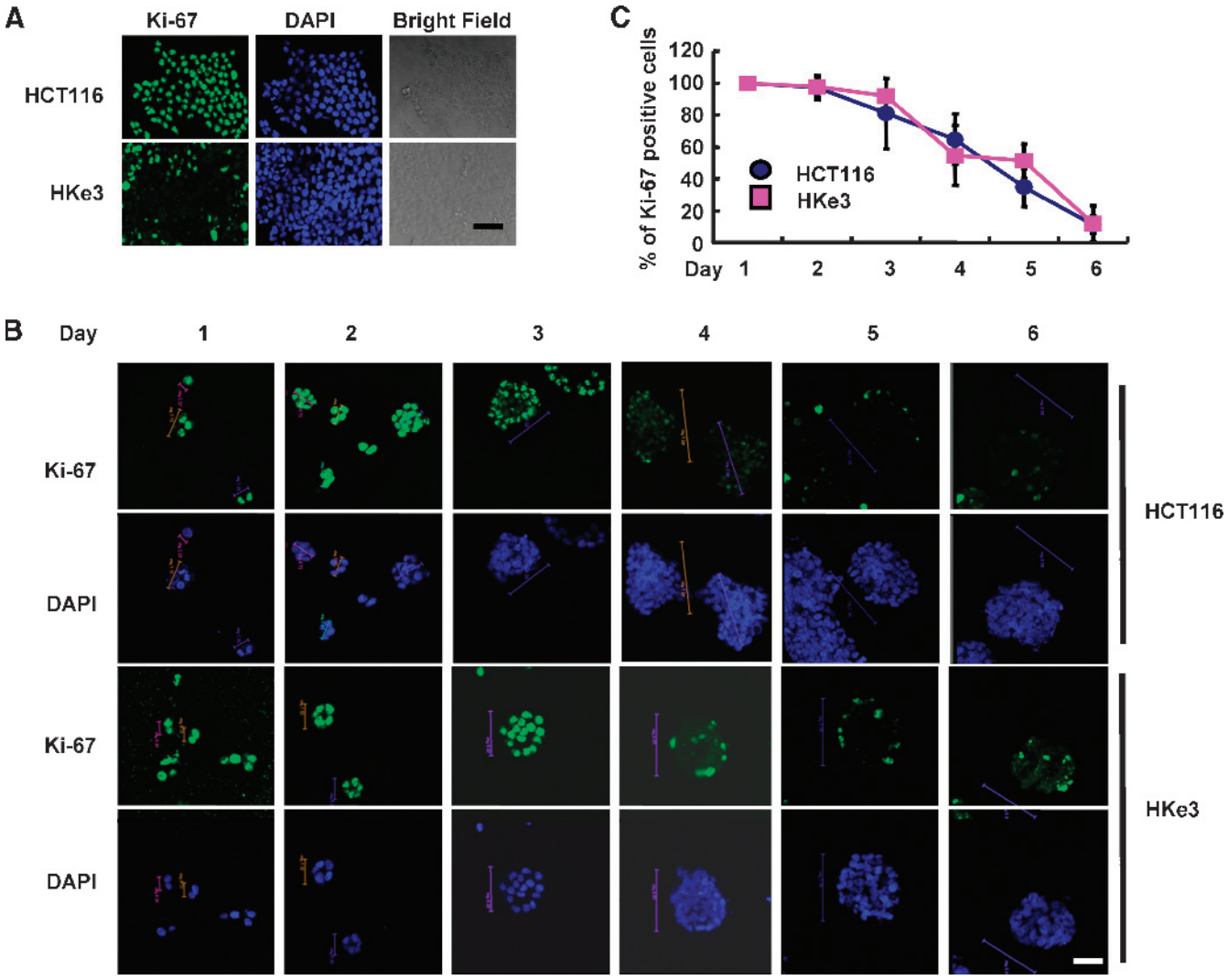

Figure 2. Cell proliferation detected by Ki-67 in the 2D and 3D cultures. (A) Ki-67 signals in HCT116 or HKe3 cells at day 6 in the 2D culture. Green, Ki-67; blue, nuclear DNA (DAPI). Bar, 50 μm. (B) Ki-67 signals in HCT116 or HKe3 cells at the indicated day from day 1 to day 6 in the 3D culture. Bright field image is also shown. Green, Ki-67; blue, nuclear DNA (DAPI). Bar, 50 μm. (C) The ratio of Ki-67–positive cells at the indicated day from day 1 to day 6 the in 3D culture. Blue circle, HCT116; purple rectangle, HKe3.

by detecting the cleaved caspase-3 signals. The ratios of apoptotic 3D structures for HCT116 and HKe3 cells were 16.9% and 80.5%, respectively (*P < .001; Figure 1*C*), indicating that apoptosis activity is present for luminal cavity epithelium in the 3D culture of HKe3 cells and is inhibited in the HCT116 cells. Furthermore, apoptosis activity in e3-MKRas#14 cells was inhibited like HCT116 cells (Figure W2*C*). These results suggest that activated KRAS suppresses apoptosis in the 3D culture.

HKe3 Cells in the 3D Culture as a Colonic Crypt Model

Continuous proliferation is one of the features of cancer cells in the traditional 2D culture. A proliferation marker Ki-67 signal for HKe3 cells grown in 2D culture was expectedly detected only in the cells located at the outer region but not at the inner region (Figure 2*A*). Conversely, the Ki-67 signal for the HCT116 cells grown in 2D culture was observed in both the inner and outer regions (Figure 2*A*). Together, these results suggest that activated KRAS suppresses the contact inhibition of cell growth in the 2D culture.

To address whether or how activated KRAS influences cell proliferation in the 3D cell culture, we examined the time course–dependent proliferation of the cells grown in the 3D culture for 6 days. Ki-67 signals were evidently detected both in the HKe3 and HCT116 3D structures from day 1 to day 3, whereas Ki-67 signals were suddenly decreased at day 4 not only in the HKe3 cells but also in the HCT116 cells (Figure 2*B*). Ki-67–positive cells in the 3D structures of HCT116 and HKe3 were similarly decreased time course–dependently, 97.1% and 97.6% at day 2, 80.8% and 91.9% at day 3, 64.7% and 54.6% at day 4, 34.4% and 51.2% at day 5, and 11.0% and 11.8% at day 6, respectively (Figure 2*C*). A significant difference in the ratio of Ki-67–positive cells between the HCT116 and HKe3 cells was not detected at any time point (P > .05; Figure 2*C*). These results, together, suggest that activated KRAS is rather involved in the inhibition of apoptosis than in cell proliferation. Of note is the decreased proliferation and luminal cavity formation in HKe3 cells in the 3D culture at day 4, as TA cells in the colonic crypt *in vivo* differentiate to TD cells at day 4 [9], suggesting that HKe3 cells in this 3D culture will be applied as a colonic crypt model.

3D-Specific Suppression of DNA Metabolism–Related Genes by Activated KRAS

To explore the differentially expressed genes regulated by activated KRAS in the 3D culture, we performed expression microarrays using HCT116 and HKe3 cells grown in the 2D or 3D culture for 6 days. Differentially expressed genes were cut off by three-fold up or three-fold down, and these are shown as a Venn diagram (Figure 3*A*), and the genes detected are listed (Tables W1–W3). Of note is the existence of 3D-specific differentially expressed genes. The numbers of 3D-specific three-fold up- and three-fold down-expressed genes were 328 and 1397, respectively (Figure 3*A*; Table W4).

To address the functions of 3D-specific downregulated genes by activated KRAS, we performed gene ontology (GO) analysis for the genes (Table W4). The significant GO for the 3D-specific downregulated genes by activated KRAS was classified into the GOs such as "DNA metabolism" (with a *P* value of 7.6e–24), "DNA repair" (*P* = 1.4e–19), "response to DNA damage stimulus" (*P* = 3.8e–18), and "cell cycle checkpoint" (*P* = 1.9e–16; Table W4*B*). However, the most significant GO for the 3D-specific upregulated genes by activated KRAS was "entrainment of circadian clock" with a *P* value of 1.1e–4 (data not shown). From the viewpoint of tumorigenesis and statistical significance, 3D-specific downregulated genes by activated KRAS are of great interest. The 3D-specific downregulated genes, including *BRCA1* [12,31–35], *BRCA2* [12,31,33,34,36,37], *EXO1* (*exonuclease-1*) [38–40], and *TP53* (*p53*) [12,34,41,42], were commonly listed among the GO categories related to "DNA metabolism," "cell cycle," "DNA repair," and "response to DNA damage stimulus" (Table W4*C*), and these four genes are known as tumor suppressor genes [1,33,38]. Interestingly, in the 2D culture, expressions of these four genes in HCT116 cells, compared with those in HKe3 cells, were 4.15-, 4.27-, 4.60- and 1.19-fold upregulated, respectively (Table W4, *A* and *D*). Furthermore, 62 of the 3D-specific downregulated 72 genes classified as "DNA metabolism" were rather upregulated in the 2D culture, indicating the opposite expression profiles for these genes between 2D and 3D cultures (Table W4*D*).

3D-Specific Suppression of TP53, BRCA1, BRCA2 and EXO-1 by Activated KRAS

We performed real-time quantitative reverse transcription–polymerase chain reaction to validate the microarray results of *BRCA1*, *BRCA2*, *EXO-1*, and *TP53*. In HKe3 cells for the 3D culture, the expression levels of *BRCA1*, *BRCA2*, *EXO-1*, and *TP53* were increased to 11.22, 6.38, 6.20, and 9.31 times, respectively (*$P < .001$) compared with HCT116 cells in the 3D culture (Figure 3*B*), suggesting that activated KRAS in the 3D culture exactly inhibits the messenger RNA (mRNA) expressions of these four genes. In the 2D culture, the expression levels of *BRCA1*, *BRCA2*, and *EXO-1* in HKe3 cells, compared with those in HCT116 cells, were decreased to 0.21, 0.28, and 0.28 times, respectively ($P < .001$), whereas *TP53* was not significantly changed in the 2D culture (1.09 times, $P = .31$; Figure 3*B*).

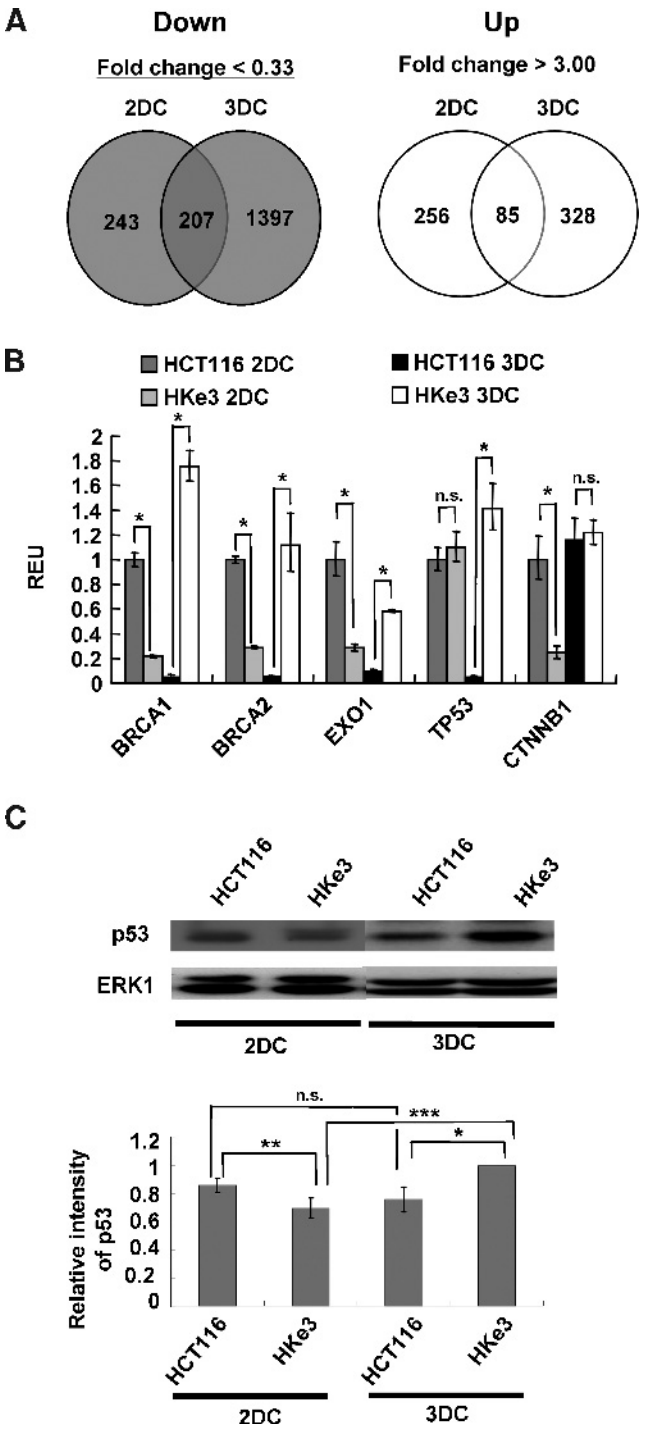

Figure 3. 3D-specific suppression of DNA repair–related tumor suppressor genes including *TP53*, *BRCA1*, *BRCA2*, and *EXO-1* by activated KRAS. (A) Differentially expressed genes detected by the expression microarray analysis. Venn diagrams show the number of genes more than three-fold down (gray circles) or three-fold up (white circles) in HCT116 cells compared with HKe3 cells in the 2D culture (2DC) and/or the 3D culture (3DC). (B) Validation of mRNA expression levels of the 3D-specific downregulated genes detected by microarray expression analysis. Each REU was normalized to *ACTB*, and REUs were determined by the REU of HCT116 in the 2D culture as 1.0. Statistical significance (*$P < .001$) exists in REUs between HCT116 in the 2D culture and HKe3 in the 3D culture. n.s., no significant difference. *CTNNB1* as control. Gray bar, HCT116 in the 2D culture; light gray bar, HKe3 in the 2D culture; black bar, HCT116 in the 3D culture; white bar, HKe3 in the 3D culture. (C) Western blot analysis of p53 in HCT116 and HKe3 cells in the 2D or 3D culture (upper). Quantitative analysis for the expression of p53 (lower). Each signal was normalized to ERK1. Relative intensities of p53 were determined by the p53 signal of HKe3 cells in the 3D culture as 1.0. *$P < .05$, **$P < .005$, ***$P < .0005$. n.s., no significant difference.

These four gene expressions in HCT116 cells in the 3D culture, compared with those in the 2D culture, were decreased to 0.05 (*BRCA1*), 0.05 (*BRCA2*), 0.09 (*EXO1*), and 0.04 (*TP53*) times, respectively ($P < .001$), whereas these gene expressions in HKe3 cells in the 3D culture, compared with those in the 2D culture, were increased to 8.11 (*BRCA1*), 3.84 (*BRCA2*), 2.03 (*EXO-1*), and 1.28 (*TP53*) times, respectively ($P < .05$). Together, these results suggest the critical roles for activated KRAS in the regulation of expression of these tumor suppressor genes.

Considering the importance of p53 in tumorigenesis, we examined p53 protein level by Western blot. Although the p53 protein level in HCT116 cells in the 2D culture, compared with HKe3 cells in the 2D culture, was slightly increased to 1.23 times ($^{**}P < .005$), p53 protein level in HCT116 cells in the 3D culture, compared with HKe3 cells in the 3D culture, was decreased to 0.75 times ($^{*}P < .05$; Figure 3*C*). Furthermore, p53 expression in HKe3 cells in the 3D culture, compared with that in the 2D culture, was increased to 1.43 times ($^{***}P < .0001$; Figure 3*C*). Together, these results suggest that the p53 protein level is increased in the 3D culture through loss of activated KRAS.

Discussion

HKe3 cells, human CRC HCT116 cells disrupted at activated *KRAS*, formed a colonic cryptlike 3D structure and showed time course–dependent proliferation and differentiation under the 3D microenvironment (Figure 4*A*). In the 3D cell culture for HKe3 cells, HKe3 cells divided like TA cells in the colonic crypt from day 1 to day 3 and displayed the polarized structures like TD cells after day 4, followed by apoptosis in luminal epithelium (Figures 1 and 4*A*). In contrast, HCT116 cells having activated *KRAS* and HKe3-derived e3-MKRas#14 cells expressing activated KRAS lost apical-basal cell polarity and apoptosis/anoikis (Figures 1 and 4*B*; Figure W2). After day 4, proliferative cells detected by Ki-67 signals were evidently decreased both in HCT116 and in HKe3 cells (Figure 2, *B* and *C*). All these results suggest that HKe3 cells in the 3D culture show the features of colonic crypt, and this 3D cell culture system will be useful for elucidating the molecular mechanisms of CRC and novel functions for activated KRAS *in vivo*.

From the viewpoint of the regulated genes by activated KRAS, DNA repair–related tumor suppressor genes, including *TP53* [1,12,34,42], *BRCA1* [12,31–35], *BRCA2* [12,31,33,34,36,37], and *EXO-1* [38–40], were downregulated in a 3D-specific manner, suggesting that activated KRAS plays critical roles in the accumulation of genetic alterations through the suppression of DNA repair genes (Figure 4*B*), and this suppression leads to the disruption of a barrier to tumor progression in precancerous lesions [43].

Because colonic crypts *in vivo* are localized in an acidic microenvironment and are continuously exposed to oxidative stress, colonic crypt cells possess higher DNA repair activity [44,45]. Cells grown in the 3D culture here might reflect microenvironment *in vivo* to react against acidic condition, culminating in an induced expression of DNA repair genes and activated KRAS might inhibit DNA repair activity, leading to the accumulation of genetic alterations. The reason why DNA repair activity is remarkable in the 3D culture, but not in the 2D culture, may reflect the difference between cellular conditions induced by microenvironments of the 2D and 3D cultures. Thus, microenvironmental conditions should be much taken into account for elucidating molecular mechanisms of cancer. In this study, we focused on interactions of epithelial cells and basement membranes in the 3D microenvironment; therefore, evaluation of other microenvironmental conditions including stroma cells should be needed for a better understanding of molecular mechanisms underlying the development of CRC *in vivo*.

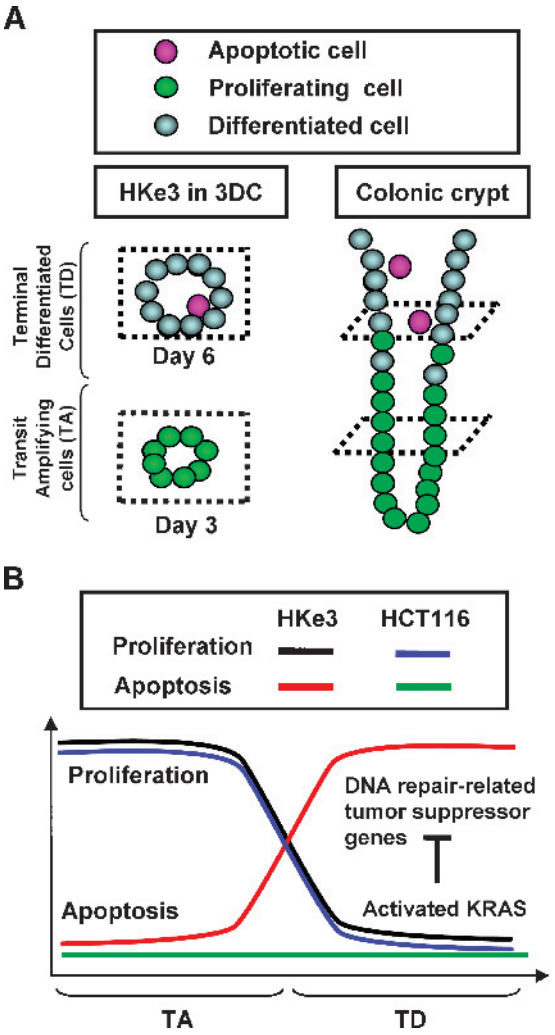

Figure 4. Critical function of activated KRAS in DNA repair–related tumor suppressor genes in the 3D colonic crypt model. (A) A schematic model of HKe3 cells in the 3D culture as colonic crypt *in vivo*. A representative model is shown at day 3 and day 6 when TA and TD cells mainly exist, respectively. Apoptotic cells are produced from TD cells in the luminal cavity. Red, apoptotic cell; green, proliferating cells; blue, differentiated cells. (B) A schematic model of apoptosis and proliferation in the colonic crypt and activated KRAS function in the inhibition of DNA repair–related tumor suppressor genes. Apoptosis and proliferation indexes are shown for HKe3 (red and black lines) and HCT116 (green and blue lines) cells. "T" sign indicates the repression of DNA repair–related tumor suppressor genes including *TP53*, *BRCA1*, *BRCA2*, and *EXO-1* by activated KRAS.

The down-regulation of DNA repair–related tumor suppressor genes was evidently detected at the mRNA level (Figure 3*B*), whereas the p53 protein level was not completely concomitant with the mRNA level (Figure 3*C*), suggesting that particular mechanisms do exist in the regulation of p53, such as protein degradation and translation regulated by microRNA [46]. Further examination of the differentially expressed

genes including microRNA and signaling on this 3D culture system will lead to a better understanding of CRC development.

Another issue in this study is that the molecular mechanisms of tumorigenesis should be reevaluated in the 3D microenvironment [2]. Most of the downregulated genes classified as "DNA metabolism" by activated KRAS in the 3D culture were rather upregulated in the 2D culture, i.e., opposite expression profiles between the 2D and 3D cultures exist (Table W4*D*). Researchers should adequately consider cell culture conditions; otherwise, molecular mechanisms of the tumorigenesis *in vivo* may be misunderstood.

We have established a 3D colonic crypt model using HKe3 cells, HCT116 cells disrupted at activated *KRAS*, and demonstrated that activated KRAS is involved in deregulation of apical-basal cell polarity, luminal cavity formation with apoptosis, and 3D-specific suppression of DNA repair–related tumor suppressor genes including *TP53*, *BRCA1*, *BRCA2*, and *EXO-1*. Activated KRAS plays critical roles in the accumulation of genetic alterations through the inhibition of DNA repair genes and apoptosis, resulting in the disruption of the barrier-to-tumor progression. Our 3D colonic crypt model will provide a useful tool for investigating the molecular mechanisms of CRC development *in vivo* and design of CRC therapies.

Acknowledgment

The authors thank T. Danno and Y. Hirose for technical assistance.

References

[1] O'Brien LE, Zegers MM, and Mostov KE (2002). Opinion: Building epithelial architecture: insights from three-dimensional culture models. *Nat Rev Mol Cell Biol* **3**, 531–537.

[2] Griffith LG and Swartz MA (2006). Capturing complex 3D tissue physiology *in vitro*. *Nat Rev Mol Cell Biol* **7**, 211–224.

[3] Birgersdotter A, Sandberg R, and Ernberg I (2005). Gene expression perturbation *in vitro*—a growing case for three-dimensional (3D) culture systems. *Semin Cancer Biol* **15**, 405–412.

[4] Bissell MJ and Labarge MA (2005). Context, tissue plasticity, and cancer: are tumor stem cells also regulated by the microenvironment? *Cancer Cell* **7**, 17–23.

[5] Yamada KM and Cukierman E (2007). Modeling tissue morphogenesis and cancer in 3D. *Cell* **130**, 601–610.

[6] Huber MA, Kraut N, and Beug H (2005). Molecular requirements for epithelial-mesenchymal transition during tumor progression. *Curr Opin Cell Biol* **17**, 548–558.

[7] Thiery JP and Sleeman JP (2006). Complex networks orchestrate epithelial-mesenchymal transitions. *Nat Rev Mol Cell Biol* **7**, 131–142.

[8] Wodarz A and Nathke I (2007). Cell polarity in development and cancer. *Nat Cell Biol* **9**, 1016–1024.

[9] McDonald SA, Preston SL, Lovell MJ, Wright NA, and Jankowski JA (2006). Mechanisms of disease: from stem cells to colorectal cancer. *Nat Clin Pract Gastroenterol Hepatol* **3**, 267–274.

[10] Cho KK and Vogelstein B (1992). Genetic alterations in the adenoma-carcinoma sequence. *Cancer* **70**, 1727–1731.

[11] Hanahan D and Weinberg RA (2004). The hallmarks of cancer. *Cell* **100**, 57–70.

[12] Vogelstein B and Kinzler KW (2004). Cancer genes and the pathways they control. *Nat Med* **10**, 789–799.

[13] Kinzler KW and Vogelstein B (1998). Colorectal tumors. In *The Genetic Basis of Human Cancer*. B Vogelstein and KW Kinzler (Eds). McGraw-Hill, New York, NY. pp. 565–587.

[14] Rosin-Arbesfeld R, Ihrke G, and Bienz M (2001). Actin-dependent membrane association of the APC tumour suppressor in polarized mammalian epithelial cells. *EMBO J* **20**, 5929–5939.

[15] Maire G, Yoshimoto M, Chilton-MacNeill S, Thorner PS, Zielenska M, and Squire JA (2009). Recurrent RECQL4 imbalance and increased gene expression levels are associated with structural chromosomal instability (S-CIN) in sporadic osteosarcoma. *Neoplasia* **11**, 260–268.

[16] Cho JY, Kim JH, Lee YH, Chung KY, Kim SK, Gong SJ, You NC, Chung HC, Roh JK, and Kim BS (1997). Correlation between K-*ras* gene mutation and prognosis of patients with nonsmall cell lung carcinoma. *Cancer* **79**, 462–467.

[17] Karapetis CS, Khambata-Ford S, Jonker DJ, O'Callaghan CJ, Tu D, Tebbutt NC, Simes RJ, Chalchal H, Shapiro JD, Robitaille S, et al. (2008). K-*ras* mutations and benefit from cetuximab in advanced colorectal cancer. *N Engl J Med* **359**, 1757–1765.

[18] Marchetti A, Milella M, Felicioni L, Cappuzzo F, Irtelli L, Del Grammastro M, Sciarrotta M, Malatesta S, Nuzzo C, Finocchiaro G, et al. (2009). Clinical implications of *KRAS* mutations in lung cancer patients treated with tyrosine kinase inhibitors: an important role for mutations in minor clones. *Neoplasia* **11**, 1084–1092.

[19] Shirasawa S, Furuse M, Yokoyama N, and Sasazuki T (1993). Altered growth of human colon cancer cell lines disrupted at activated Ki-*ras*. *Science* **260**, 85–88.

[20] Shirasawa S and Sasazuki T (2003). The impact of oncogenes on tumor maintenance. In *Oncogene-Directed Therapies*. JW Rak (Ed). Human Press, Inc, Totowa, NJ. pp. 229–243.

[21] Yu JL, May L, Lhotak V, Shahrzad S, Shirasawa S, Weitz JI, Coomber BL, Mackman N, and Rak JW (2005). Oncogenic events regulate tissue factor expression in colorectal cancer cells: implications for tumor progression and angiogenesis. *Blood* **105**, 1734–1741.

[22] Trobridge P, Knoblaugh S, Washington MK, Munoz NM, Tsuchiya KD, Rojas A, Song X, Ulrich CM, Sasazuki T, Shirasawa S, et al. (2009). TGF-β receptor inactivation and mutant *Kras* induce intestinal neoplasms in mice via a β-catenin–independent pathway. *Gastroenterology* **136**, 1680–1688.

[23] Baba I, Shirasawa S, Iwamoto R, Okumura K, Tsunoda T, Nishioka M, Fukuyama K, Yamamoto K, Mekada E, and Sasazuki T (2000). Involvement of deregulated epiregulin expression in tumorigenesis *in vivo* through activated Ki-*ras* signaling pathway in human colon cancer cells. *Cancer Res* **60**, 6886–6889.

[24] Tsunoda T, Furusato B, Takashima Y, Ravulapalli S, Dobi A, Srivastava S, McLeod DG, Sesterhenn IA, Ornstein DK, and Shirasawa S (2009). The increased expression of periostin during early stages of prostate cancer and advanced stages of cancer stroma. *Prostate* **69**, 1398–1403.

[25] Debnath J, Muthuswamy SK, and Brugge JS (2003). Morphogenesis and oncogenesis of MCF-10A mammary epithelial acini grown in three-dimensional basement membrane cultures. *Methods* **30**, 256–268.

[26] Koyanagi M, Nakabayashi K, Fujimoto T, Gu N, Baba I, Takashima Y, Doi K, Harada H, Kato N, Sasazuki T, et al. (2008). ZFAT expression in B and T lymphocytes and identification of ZFAT-regulated genes. *Genomics* **91**, 451–457.

[27] Bubner B, Gase K, and Baldwin IT (2004). Two-fold differences are the detection limit for determining transgene copy numbers in plants by real-time PCR. *BMC Biotechmol* **4**, 14.

[28] Livak KJ and Schmittgen TD (2001). Analysis of relative gene expression data using real-time quantitative PCR and the 2(–Delta Delta *C*(T)) method. *Methods* **25**, 402–408.

[29] Fujimoto T, Miyasaka K, Koyanagi M, Tsunoda T, Baba I, Doi K, Ohta M, Kato N, Sasazuki T, and Shirasawa S (2009). Altered energy homeostasis and resistance to diet-induced obesity in KRAP-deficient mice. *PLoS One* **4**, e4240.

[30] Schmelzle T, Mailleux AA, Overholtzer M, Carroll JS, Solimini NL, Lightcap ES, Veiby OP, and Brugge JS (2007). Functional role and oncogene-regulated expression of the BH3-only factor Bmf in mammary epithelial anoikis and morphogenesis. *Proc Natl Acad Sci USA* **104**, 3787–3792.

[31] Mao Z, Jiang Y, Liu X, Seluanov A, and Gorbunova V (2009). DNA repair by homologous recombination, but not by nonhomologous end joining, is elevated in breast cancer cells. *Neoplasia* **11**, 683–691.

[32] Miki Y, Swensen J, Shattuck-Eidens D, Futreal PA, Harshman K, Tavtigian S, Liu Q, Cochran C, Bennett LM, Ding W, et al. (1994). A strong candidate for the breast and ovarian cancer susceptibility gene BRCA1. *Science* **266**, 66–71.

[33] Zheng L, Li S, Boyer TG, and Lee WH (2000). Lessons learned from *BRCA1* and *BRCA2*. *Oncogene* **19**, 6159–6175.

[34] Kastan MB and Bartek J (2004). Cell-cycle checkpoints and cancer. *Nature* **432**, 316–323.

[35] Naseem R and Webb M (2008). Analysis of the DNA binding activity of *BRCA1* and its modulation by the tumour suppressor p53. *PLoS One* **3**, e2336.

[36] Wooster R, Bignell G, Lancaster J, Swift S, Seal S, Mangion J, Collins N, Gregory S, Gumbs C, and Micklem G (1995). Identification of the breast cancer susceptibility gene *BRCA2*. *Nature* **378**, 789–792.

[37] Bolderson E, Richard DJ, Zhou BB, and Khanna KK (2009). Recent advances in cancer therapy targeting proteins involved in DNA double-strand break repair. *Clin Cancer Res* **15**, 6314–6320.

[38] Schmutte C, Marinescu RC, Sadoff MM, Guerrette S, Overhauser J, and Fishel R (1998). Human exonuclease I interacts with the mismatch repair protein hMSH2. *Cancer Res* **58**, 4537–4542.

[39] Kucherlapati M, Nguyen A, Kuraguchi M, Yang K, Fan K, Bronson R, Wei K, Lipkin M, Edelmann W, and Kucherlapati R (2007). Tumor progression in Apc(1638N) mice with Exo1 and Fen1 deficiencies. *Oncogene* **26**, 6297–6306.

[40] Mimitou EP and Symington LS (2008). Sae2, Exo1 and Sgs1 collaborate in DNA double-strand break processing. *Nature* **455**, 770–774.

[41] Baker SJ, Fearon ER, Nigro JM, Hamilton SR, Preisinger AC, Jessup JM, vanTuinen P, Ledbetter DH, Barker DF, Nakamura Y, et al. (1989). Chromosome 17 deletions and *p53* gene mutations in colorectal carcinomas. *Science* **244**, 217–221.

[42] Vogelstein B and Kinzler KW (1992). p53 function and dysfunction. *Cell* **70**, 523–526.

[43] Halazonetis TD, Gorgoulis VG, and Bartek J (2008). An oncogene-induced DNA damage model for cancer development. *Science* **319**, 1352–1355.

[44] Oberreuther-Moschner DL, Rechkemmer G, and Pool-Zobel BL (2005). Basal colon crypt cells are more sensitive than surface cells toward hydrogen peroxide, a factor of oxidative stress. *Toxicol Lett* **159**, 212–218.

[45] Hong MY, Turner ND, Carroll RJ, Chapkin RS, and Lupton JR (2005). Differential response to DNA damage may explain different cancer susceptibility between small and large intestine. *Exp Biol Med* **230**, 464–471.

[46] Lee CH, Subramanian S, Beck AH, Espinosa I, Senz J, Zhu SX, Huntsman D, van de Rijn M, and Gilks CB (2009). MicroRNA profiling of *BRCA1/2* mutation-carrying and non–mutation-carrying high-grade serous carcinomas of ovary. *PLoS One* **4**, e7314.

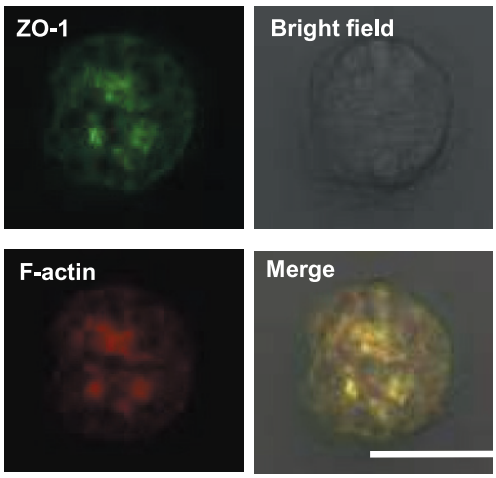

Figure W1. Apical-basal cell polarity in HKe3 cells. Green, ZO-1; red, F-actin. Bar, 25 μm.

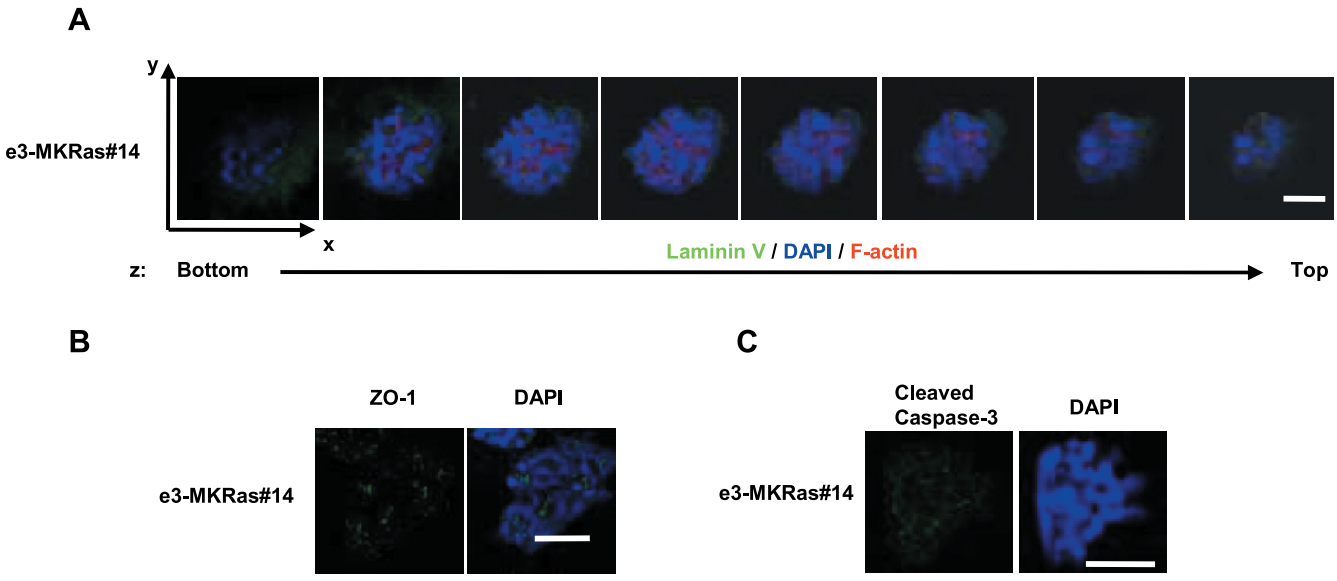

Figure W2. Loss of cell polarity, luminal cavity formation, and apoptosis in e3-mKRas#14 cells. (A) Loss of apical-basal cell polarity in e3-MKRas#14 cells. Serial cross-sectional (*x-y* plane) images of 3D spherical structures were displayed in every 3-μm distance (*z* axis). Red, F-actin; blue, nuclear DNA; green, laminin V. Bar, 25 μm. (B) Disruption of tight junctions in e3-MKRas#14 cells. Blue, nuclear DNA; green, ZO-1. Bar, 50 μm. (C) Inhibition of apoptosis in e3-MKRas#14 cells. e3-MKRas#14 cells in the 3D structures at day 6 were stained with DAPI (blue) and antibodies to the cleaved caspase-3 (green) (left). Blue, nuclear DNA; green, cleaved caspase-3. Bar, 50 μm.